

# Quantitative magnetic information from reciprocal space maps in transmission electron microscopy

Hans Lidbaum,<sup>1</sup> Ján Rusz,<sup>2,3</sup> Andreas Liebig,<sup>2</sup> Björgvin Hjörvarsson,<sup>2</sup>  
Peter M. Oppeneer,<sup>2</sup> Ernesto Coronel,<sup>4</sup> Olle Eriksson,<sup>2</sup> and Klaus Leifer<sup>4</sup>

<sup>1</sup>*Department of Engineering Sciences, Uppsala University, Box 534, S-751 21 Uppsala, Sweden*

<sup>2</sup>*Department of Physics, Uppsala University, Box 530, S-751 21 Uppsala, Sweden*

<sup>3</sup>*Institute of Physics, Academy of Sciences of the Czech Republic,  
Na Slovance 2, CZ-182 21 Prague, Czech Republic*

<sup>4</sup>*Department of Engineering Sciences, Uppsala University, Box 530, S-751 21 Uppsala, Sweden*

(Dated: April 2, 2022)

One of the most challenging issues in the characterization of magnetic materials is to obtain quantitative analysis on the nanometer scale. Here we describe how electron magnetic circular dichroism (EMCD) measurements using the transmission electron microscope (TEM) can be used for that purpose, utilizing reciprocal space maps. Applying the EMCD sum rules, an orbital to spin moment ratio of  $m_L/m_S = 0.08 \pm 0.01$  is obtained for Fe, which is consistent with the commonly accepted value. Hence, we establish EMCD as a quantitative element specific technique for magnetic studies, using a widely available instrument with superior spatial resolution.

PACS numbers: 68.37.Lp, 75.70.Ak, 78.20.Bh, 79.20.Uv

Keywords: magnetic circular dichroism, electron energy-loss spectra, transmission electron microscopy

Fast advances in the field of magnetic nanostructures, both in fundamental research and technological development, call for new magnetic characterization methods. Electron microscopy is nowadays a standard technique for structural and chemical analysis down to the atomic scale. Magnetic imaging [1] in the TEM is also possible while element-specific magnetic moments and spin-orbit ratios have until now been the domain of synchrotron based dichroic experiments, such as x-ray magnetic circular dichroism (XMCD) [2]. Although XMCD is widely applied in materials science, it is mainly related to surface measurements and with limitations in spatial resolution. The recent work of Schattschneider et al. [3] – demonstrating the applicability of dichroic effects in the TEM – opens a new route for high-resolution element specific magnetic characterization, using widely accessible standard laboratory equipment.

EMCD measurements are in principle simple. An unpolarized electron beam, passing through a magnetic material, exhibits a magnetic dichroism in the momentum resolved electron energy-loss spectra (EELS) [3]. The origin of this effect stems from the inelastic scattering of incoming high-energy electrons that excite core electrons to unoccupied states. The signal at a scattering vector  $\mathbf{k}$  contains mixed contributions of all pairs of diffracted beams with momentum transfers  $\mathbf{q}$  and  $\mathbf{q}'$ . A dichroic effect appears when two EELS-spectra – extracted at specific detector positions in reciprocal space defined by a mirror axis – are subtracted (see Fig. 1). This difference spectrum is called in the following the EMCD signal. The vector product  $\mathbf{q} \times \mathbf{q}'$ , which plays the same role in EMCD as the circular polarization in XMCD experiments [3], must have a non-zero scalar product with the direction of the magnetic moment in order to observe

a dichroic effect [4].

While the principle of EMCD has been demonstrated, decisive progress is required to allow quantitative spatially resolved magnetic analysis, which is reported here. The recent derivation of the EMCD sum rules for extraction of spin ( $m_S$ ) and orbital ( $m_L$ ) magnetic moments represents an important step in that direction [4, 5]. As EMCD relies on reciprocal space vectors, proper  $\mathbf{k}$ -space selection is essential. So far, most measurements are carried out by selecting a limited part of reciprocal space from where the EELS-spectra are acquired [3, 6]. As shown in this letter, increased flexibility for data optimization and precision in  $\mathbf{k}$ -space selection is obtained when a map showing the distribution of the signal in reciprocal space is available. Energy filtered reciprocal space maps can so far only be considered as semi-quantitative [5, 7], due to lack of data treatment. For a quantitative measurement, the signal to noise (S/N) ratio must be substantially increased and a set of procedures for data analysis of core-loss edge energy intensities must be devised. Theoretical maps of the EMCD signal provide insight into the  $\mathbf{k}$ -space dependence of the magnetic signal and provide guidance for extracting quantitative magnetic (bulk) information from experimental data.

We choose to demonstrate the technique on bcc Fe, primarily because its magnetic properties are well known, which allows for a precise exploration of the possibilities of the EMCD technique. Therefore, a Fe sample grown by UHV magnetron sputtering (texture angle of  $\pm 0.3^\circ$ ) was chosen for the analysis. Three-dimensional data sets, so called data cubes, consisting of the reciprocal  $k_x - k_y$  plane and electron energy-loss are acquired to obtain maps of the EMCD signal. The data cubes are similar to the spectrum-images introduced by Jean-

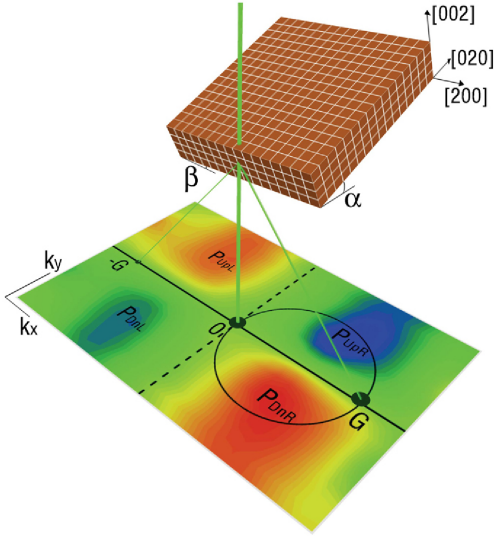


FIG. 1: A sketch of the diffraction geometry and distribution of EMCD signal in the  $k_x - k_y$  plane. The sample is tilted with respect to the incoming electron beam from a high symmetry orientation to the 2BC geometry where  $\alpha \approx 10^\circ$  and  $\beta \approx 0.4^\circ$ . In this geometry only the transmitted (0) and Bragg scattered beams ( $\mathbf{G}$ ) are strongly excited (large black spots). The optimum detector positions are indicated as  $P_{UpR}$  and  $P_{DnR}$  for 2BC geometry using a horizontal mirror axis (solid line). For the 3BC geometry,  $\alpha \approx 10^\circ$  and  $\beta = 0^\circ$ , an additional vertical mirror axis is available (dashed line). In the experiment, energy filtered diffraction patterns appear in the  $k_x - k_y$  plane; here an EMCD map is shown as a guide to the eye. The black circle indicates detector positions where  $\mathbf{q} \perp \mathbf{q}'$ , i.e. the Thales circle.

guillaume and Colliex [8], but here diffraction patterns instead of images are used. The energy filtered diffraction patterns were acquired using a post-column Gatan GIF2002 spectrometer on a FEI Tecnai F-30ST FEG operated at 300kV with energy step of 1eV (slit width 2eV) at a sample area of thickness  $19 \pm 2\text{nm}$ .

The *geometrical conditions* of the EMCD experiment will be described, as they are crucial for understanding the effect. The first EMCD experiments [3] were performed with the sample oriented in a two beam case (2BC) geometry, which is depicted in Fig. 1. The sample is tilted with respect to the incoming electron beam from a high symmetry orientation by an angle  $\alpha \sim 10^\circ$ , where mainly a row of reflections in reciprocal space, the so-called systematic row, is excited. By tilting the sample further in the perpendicular direction by a small angle of  $\beta \sim 0.4^\circ$  the 2BC geometry is obtained. In this geometry the transmitted and Bragg scattered beam  $\mathbf{G} = (200)$  in Fe are strongly excited, while all others are weak. To be able to use the sum rules [4], allowing a quantitative assessment of the  $m_L/m_S$  ratio, the dichroic signal must be extracted using *two symmetrically placed detectors* in reciprocal space and the incoming beam should lie within a mirror symmetry plane of the crystal struc-

ture. This mirror plane cuts the diffraction pattern in halves. The EMCD signal is given by the difference of a spectrum extracted in the upper half plane (at  $P_{UpR}$ ) and the corresponding spectrum in the lower half plane (at  $P_{DnR}$ ) in reciprocal space, see Fig. 1. This defines a mirror axis in reciprocal space for the 2BC geometry, denoted as *horizontal mirror axis*. By using the mirror axis and correspondingly subtracting all spectra in reciprocal space, maps of the EMCD signal (at  $L_{2,3}$  edges) are constructed. However, the 2BC geometry does not fulfill the condition of symmetric detector positions. This can be seen in Fig. 1, where the (200) atomic planes are not symmetric with respect to the positions of the detectors ( $P_{UpR}$  and  $P_{DnR}$ ), leading to limitations in the use of the 2BC geometry for  $m_L/m_S$  ratio determination. Therefore, we apply the three beam case (3BC) geometry, which is fully symmetric. Here, the incoming beam is oriented within a symmetry plane (200),  $\beta = 0^\circ$  in Fig. 1. The condition of symmetric detector positions is now fulfilled when extracting the dichroic signal as a difference in spectra between left and right half plane, defining a *vertical mirror axis*. It should be noted that the 3BC geometry also enables the use of a horizontal mirror axis, although with the same asymmetry as in the 2BC geometry. By using both mirror axes we can also construct *double difference maps*. They provide improved statistics and greatly reduced error caused by asymmetry [9].

The EMCD signal evolves as an entwined property of sample thickness and orientation due to dynamic electron diffraction effects. Thus, simulations of the EMCD experiments include both Bloch-wave simulations of dynamic scattering of the fast electrons, as well as *ab initio* calculations of the inelastic scattering in a magnetic sample [10]. Inelastic transition matrix elements were calculated including spin-orbit coupling with magnetization direction [016] as imposed by the magnetic field of the objective lens, corresponding to about  $10^\circ$  tilt of the sample. In order to simulate the finite collection angle and the relative misorientation of illuminated regions in the experiments ( $\pm 0.3^\circ$ ), maps of the EMCD signal were averaged over a set of Laue circle centers. Simulated maps of the relative EMCD signal at  $L_3$  edge for 2BC and 3BC geometries are displayed in Fig. 2a and 2e, respectively. Since DFT calculations predict a very low orbital momentum ( $\sim 0.045\mu_B$ ) in bcc Fe, the EMCD map at  $L_2$  (not shown) has a similar structure as the  $L_3$  map but with reversed sign [10]. In the 2BC geometry, the strongest dichroic signal does actually not lie on the Thales circle positions as previously assumed [3], not even for an ideal crystal. It is instead shifted toward the strongly excited reflection, denoted as  $\mathbf{G}$  in Fig. 1. A reduced EMCD signal is also present around the weakly excited reflection ( $-\mathbf{G}$ ), at positions  $P_{UpL}$  and  $P_{DnL}$  in Fig. 1.

Using the experimental data cube of energy filtered diffraction patterns, maps of the  $\mathbf{k}$ -dependent EMCD sig-

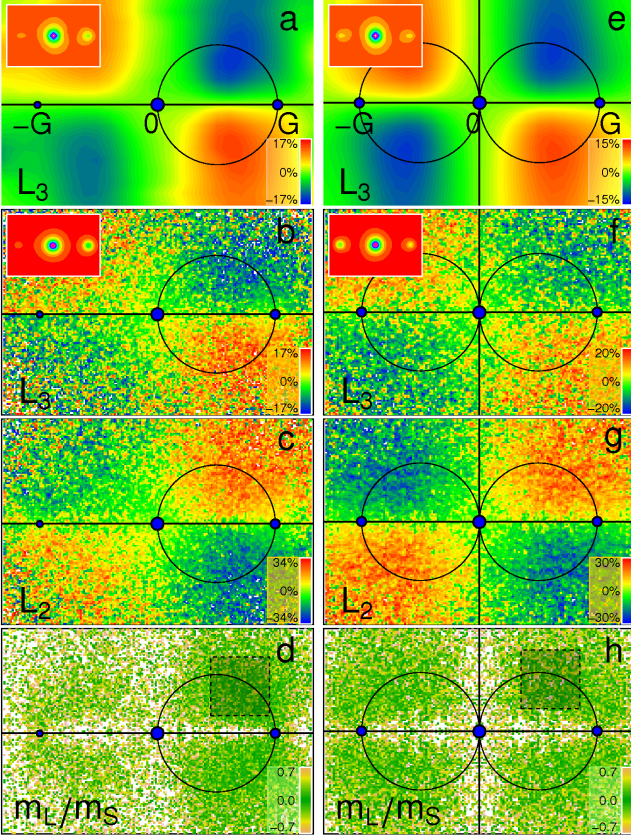


FIG. 2: Reciprocal space maps of the EMCD signal and  $m_L/m_S$  ratio for the Fe sample oriented in a 2BC geometry (left) and 3BC geometry (right). Theoretically simulated relative EMCD maps at the  $L_3$  edge are shown in a) and e), see text for details. The inset shows the simulated diffraction pattern. In b) and c) [f) and g)] for 3BC] maps of experimentally obtained relative EMCD signal at  $L_3$  and  $L_2$  edges are shown (sample thickness of  $t_{exp} = 19 \pm 2$  nm). The black lines indicate the applied mirror axes and blue spots the positions of the transmitted and Bragg scattered  $\mathbf{G} = (200)$  and  $-\mathbf{G} = (\bar{2}00)$  beams. The insets in b) and f) show the diffraction patterns averaged over an energy interval from 695 eV to 740 eV. In d) and h) the experimental  $m_L/m_S$  maps are shown, where the box indicates the region with minimal noise. Values outside the range of color bar are shown as white.

nal are constructed from the extracted spectra. Each spectrum in the  $k_x - k_y$  plane was peak fitted and the integrated  $L_{2,3}$  edge intensities are exploited to obtain the EMCD maps [9]. Peak fitting removes the need of somewhat arbitrary energy window selection for separating  $L_3$  and  $L_2$  components and corrects for eventual energy shifts due to non-isochromaticity of the spectrometer. Experimental maps of the relative EMCD signal at the  $L_{2,3}$  edges in 2BC and 3BC geometries are shown in panels b, c, f and g of Fig. 2, respectively. We find a very good correspondence between the theoretical prediction and experimental measurements regarding the position in reciprocal space and strength of the EMCD signal in

both 2BC and 3BC geometries. From the 2BC data cube two spectra were extracted using a box with the size of  $0.5\mathbf{G}_{200} \times 0.5\mathbf{G}_{200}$  at the  $P_{UPR}$  and  $P_{DnR}$ -positions (similarly to Ref. [12]) and peak fitted. In Fig. 3a the  $L_{2,3}$  edge intensities and a continuum background used in the fit of the experimental data are shown. The spectra show a clear EMCD signal with good S/N ratio. Experiment and simulation reveal a relative EMCD signal (difference divided by its sum) at the  $L_3$  edge of approx. 8% and 12%, respectively. Note that a strong EMCD signal is obtained in spite of the texture angle of  $\pm 0.3^\circ$ , which is of high importance for a practical use of EMCD. The technique is therefore robust against small distortions of the crystal orientation, allowing for the characterization of imperfect crystals. A texture angle will have a similar effect on the EMCD signal as an increase of convergence angle. A semi-convergence angle of 10 mrad corresponds in the TEM used here to a probe size of about 0.13 nm [11]. Here, we show that a quantitative EMCD signal is obtainable at deviations in the relative sample to probe orientation of  $\pm 5\text{mrad}$ . Therefore, the approach demonstrated here, has the potential for sub-nanometer resolution. The quest to reach the ultimate resolution of this technique will thus not be dominated by the achievable convergence angle or electron probe size, but by the stability of the sample and the electron microscope itself.

A quantitative assessment of spin and orbital angular momenta can be obtained from the EMCD sum rules [4, 5]. Correspondingly, a map of the  $m_L/m_S$  ratio is obtained by calculating at each position in reciprocal space:

$$\frac{m_L}{m_S} = \frac{2 \int_{L_3} \Delta I(E) dE + \int_{L_2} \Delta I(E) dE}{3 \int_{L_3} \Delta I(E) dE - 2 \int_{L_2} \Delta I(E) dE} \quad (1)$$

with  $\Delta I(E) = I(P_i) - I(P_j)$  where  $I(P_i)$  and  $I(P_j)$  are the EELS-spectra extracted at the two detector positions, e.g. in the 2BC geometry a choice of  $P_i = P_{UPR}$  implies using  $P_j = P_{DnR}$  as indicated in Fig. 1. The general sum rule expressions [4] predict a  $\mathbf{k}$ -independent  $m_L/m_S$  ratio, i.e. the intensity of a large part of reciprocal space can be employed to determine the ratio. Nevertheless, the S/N ratio should be optimized by selecting the region in reciprocal space with highest EMCD signal. Since sum rules involve several approximations and assumptions, which may not be perfectly fulfilled, we evaluated theoretical  $m_L/m_S$  maps (not shown). They reveal the effect of 2BC asymmetry, which becomes non-negligible well outside the Thales circle. In the 3BC geometry even a deviation as small as  $\beta = 0.05\mathbf{G}_{200}$  can introduce substantial variations of the observed  $m_L/m_S$  ratio throughout the diffraction plane. Detailed calculations have shown that construction of the double difference map is a very efficient method for correcting these inaccuracies [9].

The maps enable an accurate determination of the  $m_L/m_S$  ratio. A selection window is used in the maps of the  $m_L/m_S$  ratio from which the values of all individual pixels are extracted, thus optimizing the S/N ratio.



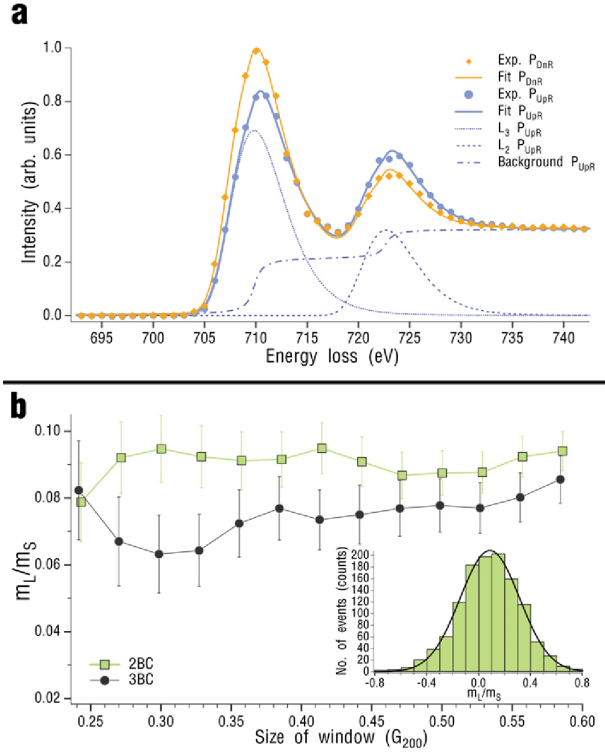


FIG. 3: Experimental EELS-spectra at Fe  $L_{2,3}$  edges and  $m_L/m_S$  ratios as a function of collection window size in  $m_L/m_S$  ratio maps. The two spectra in a) were extracted from the experimental data cube with the sample in 2BC geometry at the  $P_{DnR}$  (orange squares) and  $P_{UpR}$  positions (blue circles), averaging over  $0.5G_{200} \times 0.5G_{200}$  in reciprocal space. The different contributions to the fit function for the spectrum at the  $P_{UpR}$  position are shown. Resulting fit functions are indicated as solid lines. b)  $m_L/m_S$  ratio obtained for different window sizes in 2BC geometry using horizontal mirror axis and in 3BC using both horizontal and vertical mirror axes (double difference). Inset shows the histogram with fit of  $m_L/m_S$  ratio for the window size of  $0.5G_{200} \times 0.5G_{200}$  in 2BC orientation (indicated in Fig. 2d).

The overall  $m_L/m_S$  ratio for a given window size (collection angles) is obtained by fitting the histogram of the individual  $m_L/m_S$  values with a Gaussian (see inset in Fig. 3b). The ratio is determined as the center of the Gaussian fit. Plotting the  $m_L/m_S$  ratio as a function of the window size, a close to constant value in the  $m_L/m_S$  ratio is reached when the size of the box is sufficient to reduce the statistical fluctuations. If the window gets too large, regions with low EMCD signal are included which increase the standard deviation of the  $m_L/m_S$  ratio. Regions of minimal noise in the experimental  $m_L/m_S$  maps (indicated in panels d and h of Fig. 2) correlate with local maxima found in the EMCD maps. These results agree well with findings in Ref. [12], although here we apply the integration window numerically on the  $m_L/m_S$  ratio rather than on maps of the EMCD signal. In this way we have a better control over regions influenced by

asymmetry of the experimental geometry. Here, an optimum size of the window in reciprocal space is typically  $0.5G_{200} \times 0.5G_{200}$ . We obtain a consistent  $m_L/m_S$  ratio, depicted in Fig. 3b, of  $0.09 \pm 0.01$  in the 2BC and  $0.08 \pm 0.01$  in 3BC geometry using the double difference maps. The standard error  $\pm 0.01$  was estimated using the individual  $m_L/m_S$  ratios within the selection window.

Our experimental  $m_L/m_S$  ratio for bcc Fe is  $0.08 \pm 0.01$ , which is of the same size as that measured by other experimental techniques. The most commonly accepted values of the ratio is obtained by XMCD and gyromagnetic ratio measurements to 0.043 [13] and 0.044 [14], respectively. One may observe that the present value is somewhat larger. However, an analysis of magnetic form factors, from neutron scattering experiments, gives a value closer to the presently obtained value, namely 0.062 [15]. For bcc Fe the orbital moment is small and it is not surprising that this extremely delicate property shows a slight dispersion, depending on experimental technique or sample preparation. In this connection it is important to note that with e.g. XMCD, values of 0.043 [13], 0.07 [16], 0.085 [17] and  $0.12 \pm 0.05$  [18] for the  $m_L/m_S$  ratio have been reported for bcc Fe. In the experiments presented here, oxygen is most likely present in the vicinity of one of the Fe surfaces of the prepared TEM sample, which may influence the  $m_L/m_S$  ratio. In addition, the  $m_L/m_S$  ratio depends on the normalization of the spectra. This subject needs further investigation, though we could already confirm a minimized influence of the normalization in the ideal 3BC geometry [9]. It should be noted that one previous EMCD experiment [5] measuring the  $m_L/m_S$  ratio has been conducted for Fe. Although the ratio extracted from that work is close to ours, the analysis of reference [5] lacked clearly a quantitative data treatment, as they state explicitly. The spectra of reference [5] were not processed (e.g. peak fitted) and the S/N ratio was too low to give an accurate value.

Experimental and theoretical maps of the EMCD signal in reciprocal space are shown to agree well for the investigated sample geometries. Asymmetry problems are solved by the introduction of a new geometry, the 3BC geometry. A deviation from perfect 3BC geometry is successfully compensated using the double difference method. Application of this method yields  $m_L/m_S$  ratios of bcc Fe close to the commonly accepted value. Our work establishes therefore the quantitative use of EMCD, which, together with the high spatial resolution available in modern TEMs promises unique possibilities for truly nano-scale magnetic studies.

The work was supported through the Swedish Research Council (VR), Knut and Alice Wallenberg foundation (KAW), Göran Gustafsson foundation, STINT and computer cluster DAVID of IOP ASCR (AVOZ10100520).

- 
- [1] A. Hubert, R. Schäfer, *Magnetic Domains - The analysis of magnetic microstructures*, Springer, Berlin, 1998.
- [2] J. Stöhr et al., *Science* **259**, 658 (1993).
- [3] P. Schattschneider et al., *Nature* **441**, 486 (2006).
- [4] J. Ruzs et al., *Phys. Rev. B* **76**, 060408(R) (2007).
- [5] L. Calmels et al., *Phys. Rev. B* **76**, 060409(R) (2007).
- [6] P. Schattschneider et al., *Ultramic.* **108**, 433 (2008).
- [7] B. Warrot-Fonrose et al., *Ultramic.* **108**, 393 (2008).
- [8] C. Jeanguillaume, C. Colliex, *Ultramic.* **28**, 1 (1989).
- [9] H. Lidbaum et al., to be published.
- [10] J. Ruzs, S. Rubino, P. Schattschneider, *Phys. Rev. B* **75**, 214425 (2007).
- [11] D. O. Klenov et al., *Phys. Rev. B* **76**, 014111 (2007).
- [12] J. Verbeeck et al., *Ultramic.*, in press.
- [13] C. T. Chen et al., *Phys. Rev. Lett.* **75**, 152 (1995).
- [14] R. A. Reck, D. L. Fry, *Phys. Rev.* **184**, 492 (1969).
- [15] M. B. Stearns, *Landolt-Börnstein Numerical Data and Functional Relationships in Science and Technology*, (Springer, Berlin, 1986), Group 3, Vol. 19, Pt. a , p.53.
- [16] W. L. O'Brien et al., *J. Appl. Phys.* **76**, 6462 (1994).
- [17] D. Arvanitis et al., in *Lecture Notes in Physics* (Springer, Berlin/Heidelberg, 1996), vol. 466, pp. 145-157.
- [18] O. Zaharko et al., *Eur. Phys. J. B* **23**, 441 (2001).